Unwinding DNA strands by Single-Walled Carbon Nanotubes: Molecular docking and MD simulation approach

Ghazal Borhan, Mehdi Sahihi

Unwinding DNA strands by Single-Walled Carbon Nanotubes: Molecular docking and MD simulation approach

Ghazal Borhan, Mehdi Sahihi*

Université Clermont Auvergne, CNRS, Clermont Auvergne INP, Institut de Chimie de Clermont-Ferrand, F-63000 Clermont-Ferrand, France

***Corresponding author**

Mehdi Sahihi

Université Clermont Auvergne, France

Email: mehdi.sahihi@uca.fr

Tel.: +33(0)473407384

Abstract

Despite the growing research into the use of carbon nano-tubes (CNTs) in science and medicine, concerns about their potential toxicity remain insufficiently studied. This study utilizes molecular docking calculations combined by molecular dynamics simulations to investigate the dynamic intricacies of the interaction between single-walled carbon nanotubes (swCNTs) and double-stranded DNA (dsDNA). By examining the influence of swCNT characteristics such as length, radius, and chirality, our findings shed light on the complex interplay that shapes the binding affinity and stability of the dsDNA-swCNT complex. Molecular docking results identify a zigzag swCNT, with a radius of 0.16 Å and a length of 38 Å, as exhibiting the highest binding affinity with dsDNA (-23.9 kcal/mol). Comprehensive analyses, spanning docking results, binding energies, RMSD, radius of gyration, and potential of mean force (PMF) profiles, provide a detailed understanding of the denaturation dynamics. The PMF profiles reveal the thermodynamic feasibility of the DNA-CNT interaction, outlining distinct energy landscapes and barriers: when the selected swCNT binds within the dsDNA groove, the system becomes trapped at the first and second local energy minima, occurring at 1.48 nm and 1.00 nm, respectively. Intramolecular hydrogen bond calculations show a significant reduction, affirming the denaturing effect of swCNTs on DNA. Furthermore, the study reveals a significant reduction in the binding affinity of Ethidium Bromide (EB) to dsDNA following its interaction with swCNT, with a decrease in EB binding to dsDNA of approximately 13.2%. This research offers valuable insights into the toxic effects of swCNTs on dsDNA, contributing to a rationalization of the cancerous potential of swCNTs.

Keywords: Carbon nanotubes, DNA interaction, Molecular dynamics, Molecular docking, Nanotoxicity.

1. Introduction

Carbon nanotubes (CNTs), particularly single-walled carbon nanotubes (swCNTs), hold vast potential for applications in medicine, electronics, and materials science due to their unique mechanical, electrical, and thermal properties [1]. However, concerns regarding their biocompatibility and potential toxicity remain significant barriers to their widespread use, particularly in biomedical applications [2]. While several studies have explored the toxic effects of CNTs on organs such as the lungs, liver, and kidneys [3, 4], the precise mechanisms underlying their interaction with key biomolecules like DNA are still poorly understood. Understanding how CNTs interact with DNA is crucial, as such interactions may lead to genomic instability, a precursor to cancer and other diseases [5, 6, 7].

In recent years, several studies have attempted to elucidate the toxicological profile of swCNTs, focusing primarily on their cellular uptake and cytotoxic effects. For instance, swCNTs have been shown to penetrate cellular membranes via energy-dependent endocytosis [8], where they may induce reactive oxygen species (ROS) generation and disrupt cellular function [9]. Some studies suggest that the physical properties of swCNTs, such as length and radius, play a crucial role in modulating these effects [9]. Shorter swCNTs, with lengths between 0.5–2 μm, were found to exhibit greater toxicity compared to longer swCNTs, possibly due to their higher mobility and reduced aggregation [10]. Despite these advances, a critical gap remains: the interaction of swCNTs with genetic material, specifically double-stranded DNA (dsDNA), is yet to be comprehensively studied.

Previous research has hinted at the potential for swCNTs to enter the cell nucleus and interact with DNA, especially during mitosis when the nuclear membrane is temporarily disassembled [11, 12, 13]. While there have been some experimental efforts to detect swCNTs in nuclear spaces [11],

much of this research has been limited by the challenges of visualizing and tracking swCNTs within biological systems. More importantly, few studies have systematically explored how swCNTs may interact with dsDNA at a molecular level, leaving the genomic implications of such interactions largely speculative [14, 15, 16].

Recent advances in computational techniques, such as molecular dynamics (MD) simulations and molecular docking, offer powerful tools to investigate these interactions in silico. MD simulations, in particular, have proven effective in studying the dynamic behavior of biomolecules and their interactions with nanomaterials [17, 18, 19, 20]. Several studies have successfully utilized MD simulations to examine swCNT interactions with proteins and lipid membranes, revealing structural perturbations and potential functional consequences [21, 22]. However, there is still a notable lack of computational work focused on the interaction between swCNTs and dsDNA, despite the critical importance of understanding such interactions for assessing the genotoxic potential of CNTs.

In this study, we aim to address this gap by investigating the interaction between swCNTs and dsDNA using a combination of molecular docking and MD simulations. Our study focuses on key structural parameters of swCNTs, such as length, radius, and chirality, to elucidate their influence on binding affinity and dsDNA structural stability. By exploring the dynamic interaction between swCNTs and dsDNA, we seek to provide a detailed understanding of how these nanomaterials may induce DNA damage, thereby contributing to genomic instability. Additionally, we extend our analysis to examine how swCNT-induced structural changes in dsDNA may affect the binding affinity of small ligands, such as ethidium bromide, further shedding light on the broader biological implications of swCNT exposure.

This comprehensive approach offers significant advancements over previous studies by providing molecular-level insights into the interaction between dsDNA and swCNTs. The findings from this work will contribute to the growing body of knowledge on nanomaterial toxicity and may have important implications for the safe design and application of CNTs in biomedical fields.

2. Computational Procedure

2.1. Molecular Docking

We conducted molecular docking to elucidate the interactions between various types of swCNTs – both zigzag and armchair configurations – and dsDNA. The design of swCNTs was intricately tailored to the dimensions and size of dsDNA, relying on insights derived from X-ray crystallography data. Utilizing the crystal structure of DNA (PDB ID: 423D) obtained from the Brookhaven Protein Data Bank (www.rcsb.org), as a model dsDNA structure, we accounted for the two antiparallel strands forming a minor groove and a major groove adjacent to the base pairs, potentially serving as binding sites.

A total of 132 swCNTs were designed, incorporating different lengths, radii and chirality. These were strategically placed on the major and minor grooves based on their dimensions. The swCNTs were constructed using the nanotube builder in VMD 1.9.3 software [23] (Table 1). The study further assessed the influence of the surface area and chirality of swCNTs in these molecular interactions.

Table 1: Charasteristics of the studied swCNTs.

swCNT type	**Zigzag**						**Armchair**					
swCNT length (Å)	5	10	15	20	30	38	5	10	15	20	30	38
swCNT chirality	m=0; n=3-17						m=n=3-10					

For molecular docking simulations, we employed AutoDock4 [24], a robust molecular modeling software renowned for its efficacy in protein-ligand docking. The swCNT–dsDNA complexes were generated using AutoDockTools 1.5.6, employing the Genetic Algorithm-Local Search (GA-LS) docking, also known as the Lamarckian Genetic Algorithm (LGA) [25]. Also, the accuracy of AutoDock4 was checked by redocking the Gamma-Oxapentamidine to dsDNA. After docking the Gamma-Oxapentamidine back into dsDNA, the RMSD value between docked Gamma-Oxapentamidine and reference Gamma-Oxapentamidine was 2.4 Å and the interactions between docked Gamma-Oxapentamidine and dsDNA were like those of original modes, suggesting that AutoDock4 is suitable for docking of ligands to dsDNA.

In the docking process, designed swCNTs were treated as rigid ligands. Missing hydrogen atoms, encompassing both polar and non-polar ones, were added, and Gasteiger charges were incorporated into the .pdb input files. Auto Grid was utilized to calculate grids, employing a blind docking approach with 126 lattice points along X, Y, and Z axes, maintaining a default value of 0.375 Å between grid points – approximately a quarter of the length of a carbon-carbon single bond. Each docking simulation consisted of 100 repetitions, with 25,000,000 energy evaluations conducted for each run.

2.2. MD Simulations

We initiated MD simulations for both dsDNA in water and the dsDNA-swCNT complex, selecting the latter based on the most negative binding energy obtained from AutoDock results. For dsDNA alone simulation, the simulation box dimensions were set to 5.3 × 5.3 × 5.3 nm^3 along the X, Y, and Z axes. In the case of the dsDNA-swCNT complex, the dimensions were adjusted to 5.9 × 5.3

× 6.7 nm^3 along X, Y, and Z axes. We maintained a minimum distance of 1.0 nm between the dsDNA surface and the simulation box, and periodic boundary conditions (PBC) were applied in all three directions. The simulation boxes were solvated with TIP3P water molecules [26], and 22 sodium ions were added to neutralize the system with total charge of -22.0. The subsequent energy minimization employed the Conjugate Gradient (CG) method, setting the convergence criteria at 1×10^{-6} kJ mol^{-1} for energy difference and 1×10^{-6} kJ mol^{-1} nm^{-1} for RMS force.

Following energy minimization, systems underwent equilibration using both the NVT and NPT ensembles for 1 ns. The Nose-Hoover thermostat [27] with a damping constant of 0.2 ps and the Parrinello–Rahman barostat were applied during these equilibration steps [28, 29].

Finally, a production MD simulation was conducted for 250 ns under constant pressure (1 bar) and temperature (300 K). While the physiological temperature is approximately 310 K, the small difference between 300 K and 310 K is not expected to significantly alter the general behavior or trends in the dsDNA-swCNT interaction. This is supported by previous research showing that minor variations in temperature, are unlikely to drastically affect the structural and dynamic properties of dsDNA. Importantly, these temperatures are far below dsDNA's melting temperature (around 76°C), where significant structural changes would occur. [30] A 9Å cut-off was implemented for van der Waals and Coulomb interactions. Long-range electrostatics and constraints were addressed using the particle mesh-Ewald (PME) method [31, 32] and the LINCS algorithm [33], respectively. The MD simulations were executed using the GROMACS 2021.6 package [34, 35, 36, 37], employing the "AMBER99" force field [38] for all MD studies.

2.3. Potential of mean force (PMF) Calculations

To quantitatively assess the interaction energy of the swCNT and dsDNA, we conducted Potential of Mean Force (PMF) calculations. The final configuration of the MD simulation, achieved at equilibrium and before production run, served as the initial state for subsequent steered MD (SMD) simulations. During the SMD simulations, a force was applied along the z-dimension of the simulation box.

For the SMD simulations, we opted for a spring constant of 1000 kJ mol^{-1} nm^{-2} and a pull rate of ±0.01 nm ps^{-1}. These parameters were carefully chosen to ensure a controlled and systematic exploration of the interaction between the swCNT and dsDNA.

To capture the energetics of the system across the relevant reaction coordinate, configurations for Umbrella Sampling (US) were generated. A spacing window of 0.05 and a total distance of 2.5 nm between the center of mass of the swCNT and the dsDNA were employed. Each umbrella sampling window underwent a 1 ns equilibration period followed by a 10 ns NPT production run, utilizing a 1000 kJ mol^{-1} nm^{-2} umbrella potential to maintain the desired distance between the swCNT and dsDNA.

The Gibbs free energy profile, a key output of the PMF calculations, was constructed using the Weighted Histogram Analysis Method (WHAM). Within GROMACS, the WHAM module [39] was integrated to robustly analyze the collected data from the umbrella sampling simulations. This methodological approach allowed for a comprehensive understanding of the free energy landscape associated with the swCNT-dsDNA interaction.

3. Results and Discussion

3.1. Docking Structures Evaluation

This study delves into the intricate molecular docking interactions between armchair and zigzag swCNTs and dsDNA. Our primary objective is to unravel how the length, radius, and chirality of swCNTs shape their binding affinity with dsDNA.

Figure 1 and Tables S1 and S2 provide a comprehensive overview of the binding energy variations for both armchair and zigzag swCNTs with varying radii and lengths during the docking simulations. These results emphasize the pivotal role of swCNT characteristics in determining the strength of their interactions with dsDNA.

For armchair swCNTs with radii ranging from 0.20 to 0.54 Å, a compelling correlation between surface area and binding energy was observed. Larger surface areas consistently yielded more favorable (negative) binding energies, indicative of stronger interactions with dsDNA (Figures S1-S4). This trend can be attributed to the increased contact area between the nanotube and the dsDNA, which allows for more extensive van der Waals interactions and potentially better π-π stacking interactions. These factors collectively enhance the overall binding affinity, making the interaction more thermodynamically favorable as the surface area increases.

However, intriguing observations emerged for swCNTs with larger radii, specifically 0.61 and 0.68 Å. In these instances, where the swCNT radius surpasses the available space in the major groove of dsDNA, an unexpected behavior surfaced. When swCNTs possess a radius greater than what the major groove can accommodate, steric hindrance becomes a critical factor. The major groove of dsDNA typically has dimensions that allow for the insertion of ligands or interacting species, but when the swCNT radius surpasses these dimensions, the nanotube cannot fit optimally within the groove. This restricted spatial configuration likely leads to a reduction in the effective binding area and, consequently, lower binding affinity. Notably, for swCNTs with a radius of 0.68 Å, an inverse effect was noted, suggesting that an oversized swCNT may impede or even diminish the

binding affinity. Indeed, this observation underscores the notion that there is a threshold beyond which the physical dimensions of the swCNT become detrimental to binding. Oversized swCNTs may not only face steric hindrance but also induce unfavorable steric interactions or steric clashes with the dsDNA backbone, further contributing to the reduction in binding affinity.

Furthermore, the results show that increasing the length of the swCNT exhibited minimal impact on binding affinity. This observation can be attributed to the nature of the interaction site. While a longer swCNT may offer a larger surface area, if it cannot be positioned effectively within the major groove, the additional surface area does not translate to enhanced binding. Essentially, the inability of the swCNT to properly engage with the dsDNA due to spatial constraints limits the potential for productive interactions, such as π-π stacking or hydrogen bonding, which are crucial for strong binding affinity.

Similar behaviors were observed for zigzag swCNTs. For zigzag swCNTs with radii ranging from 0.12 to 0.55 Å, a correlation between surface area and binding energy was evident. Larger surface areas correlated with more favorable binding energies, indicative of stronger interactions with dsDNA (Figure S5-S11).

However, interesting observations also surfaced for zigzag swCNTs with larger radii, specifically 0.63 and 0.67 Å. Analogous to the armchair swCNTs, in cases where the swCNT radius exceeded the available space in the major groove of dsDNA, an unexpected behavior was observed. Increasing the swCNT length (surface area) displayed minimal impact on binding affinity.

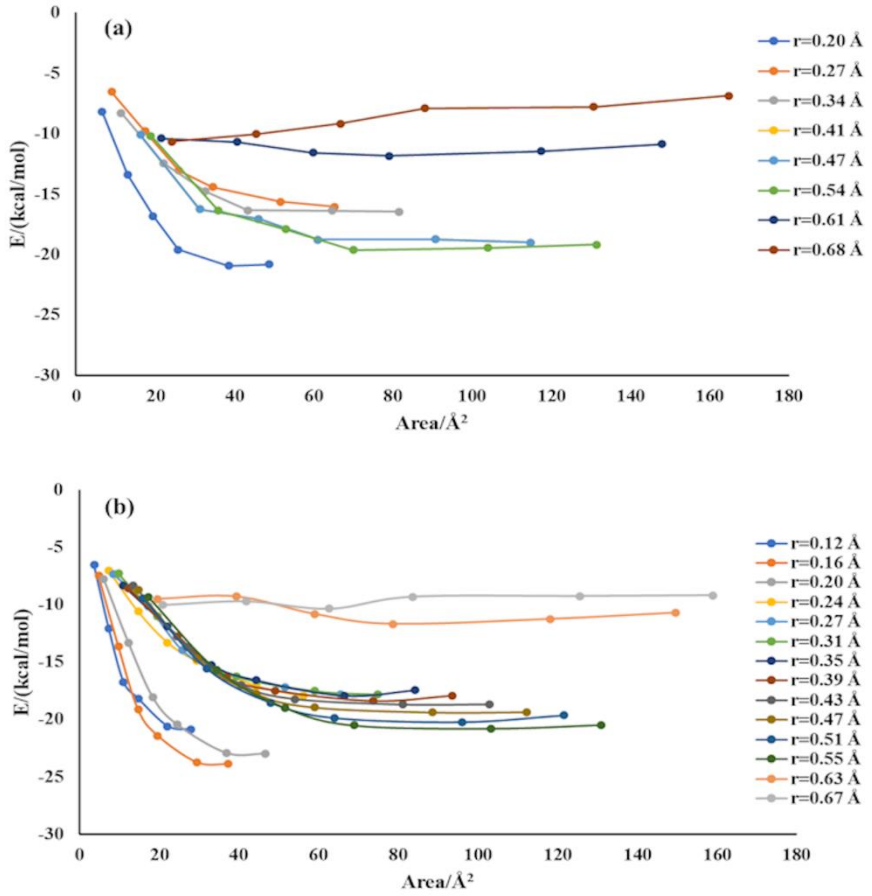

Figure 1: dsDNA binding energy variations for both (a) armchair and (b) zigzag swCNTs with varying radius and surface area of swCNT during the docking simulations.

Although the geometries of armchair and zigzag swCNTs differ, several underlying factors contribute to their comparable interaction characteristics: i) Zigzag swCNTs, like armchair swCNTs, possess unique surface properties that influence their interaction with dsDNA. The arrangement of carbon atoms in zigzag swCNTs results in a distinct electronic structure and curvature that can interact with the π-electron cloud of the DNA bases. However, the effectiveness of these interactions is highly dependent on the nanotube's dimensions, particularly its radius. When the radius of zigzag swCNTs exceeds the available space in the major groove of dsDNA, similar steric hindrances and binding challenges arise as with armchair swCNTs. ii) The geometric

compatibility of zigzag swCNTs with the dsDNA major groove is crucial. If the radius of the zigzag swCNT is too large, it may not fit comfortably within the groove, leading to suboptimal binding interactions. As observed with the armchair swCNTs, an oversized zigzag variant may not only hinder effective binding due to steric clashes but could also lead to a decrease in overall binding affinity due to the same principles of spatial restrictions. iii) Although both armchair and zigzag configurations exhibit analogous behavior in terms of steric hindrance and binding affinity, the specific electronic and structural properties attributed to their chirality can result in variations in the nature of interactions. For example, zigzag swCNTs may have different electronic interactions compared to armchair swCNTs, potentially leading to subtle differences in binding dynamics. However, when faced with excessive dimensions, these factors may become secondary to the primary concern of spatial compatibility. iv) Furthermore, the intriguing observation that zigzag swCNTs exhibit higher affinities than armchair swCNTs, despite similar radii, warrants careful consideration. This difference in affinity could stem from the distinct structural characteristics associated with zigzag swCNTs, influencing their interaction dynamics with dsDNA. The altered geometric features of zigzag swCNTs may contribute to a more favorable alignment or enhanced molecular recognition within the dsDNA binding site. Overall, the similar behaviors observed in zigzag swCNTs illustrate the fundamental principles of size and shape compatibility that govern the interaction between carbon nanotubes and dsDNA. This reinforces the need for a careful design of swCNTs, considering both their geometric and electronic properties to optimize their interactions with biological macromolecules for applications in nanomedicine and biotechnology.

Importantly, our final results highlight the zigzag swCNT with a radius of 0.16 Å and a length of 38 Å as exhibiting the highest binding affinity (-23.9 kcal/mol; Figure 2). This exceptional affinity

prompts us to conduct MD simulations to unravel the molecular and atomic details governing the dynamic behavior of the swCNT-dsDNA complex during their interaction.

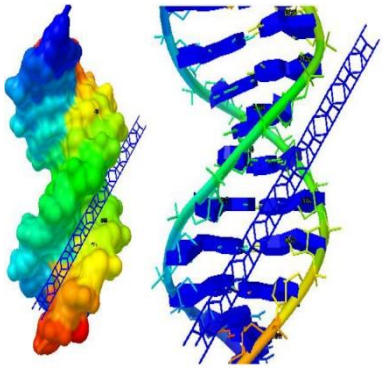

Figure 2: Docking pose of the zigzag swCNT with a radius of 0.16 Å and a length of 38 Å on the structure of dsDNA.

3.2. MD Simulations

3.2.1. Conformational and structural changes of dsDNA

To gain deeper insights into the dynamic behavior of the swCNT-dsDNA complex, we conducted a comprehensive MD simulation, focusing on the configuration derived from the highest binding energy obtained during docking. Specifically, the zigzag swCNT with a radius of 0.16 Å and a length of 38 Å was chosen for an extensive MD simulation lasting 250 ns.

The MD simulation trajectories of the swCNT-dsDNA system were meticulously analyzed alongside those of the dsDNA in water, serving as a reference system. This comparative analysis aimed to unveil the dynamic interactions within the complex and discern the impact of swCNT binding on the structural features of the dsDNA.

To comprehensively analyze the configuration changes of dsDNA molecules during the simulation process, we calculated the root mean square deviation (RMSD) and radius of gyration (Rg) of the DNA atoms relative to the crystal structure. These metrics were employed to assess the overall stability of the dsDNA structure in the presence of the swCNT.

As depicted in Figure 3a, the average RMSD values were 0.42 ± 0.08 nm in the reference simulation and 0.88 ± 0.07 nm in the dsDNA-swCNT simulation. The noticeable increase in RMSD in the dsDNA-swCNT simulation suggests substantial conformational changes induced by the denaturing effect of the swCNT. Furthermore, post approximately 130 ns, the RMSD values exhibited oscillations around their mean values without substantial changes. This stabilization in the RMSD values indicates that the configuration of dsDNA tended to reach a stable state during this period. The dynamic equilibrium observed after 130 ns suggests that the denaturation induced by the swCNT reached a point of stability, where the dsDNA structure adapted to the presence of the nanotube.

In addition to RMSD analysis, we calculated the Rg to gain further insights into the compactness and overall structural changes in the dsDNA during the simulation process. The Rg values in the dsDNA-swCNT simulation were consistently lower than those observed in the dsDNA in water system (Figure 3b).

The Rg trends reveal that both systems reached equilibrium after approximately 130 ns of trajectory, with mean values in the equilibration phase stabilizing at about 1.34 ± 0.02 nm and 1.40 ± 0.02 nm for the dsDNA-swCNT and dsDNA in water systems, respectively. This observation indicates that the compactness of both systems is relatively similar, suggesting a comparable overall structural arrangement.

The fluctuations in Rg values for the dsDNA-swCNT system, in conjunction with stabilized RMSD values, underscore the dynamic nature of the dsDNA-swCNT interaction. These observations collectively suggest that, although the compactness of both systems appears almost similar, the swCNT induces dynamic adjustments in the dsDNA structure, leading to a denaturation effect. Furthermore, we investigated the intramolecular hydrogen bonds between the two strands of dsDNA throughout the simulation process (Figure 3c). The results revealed a significant decrease in the number of intramolecular hydrogen bonds in the presence of the swCNT, providing additional evidence for the denaturation effect induced by the nanotube.

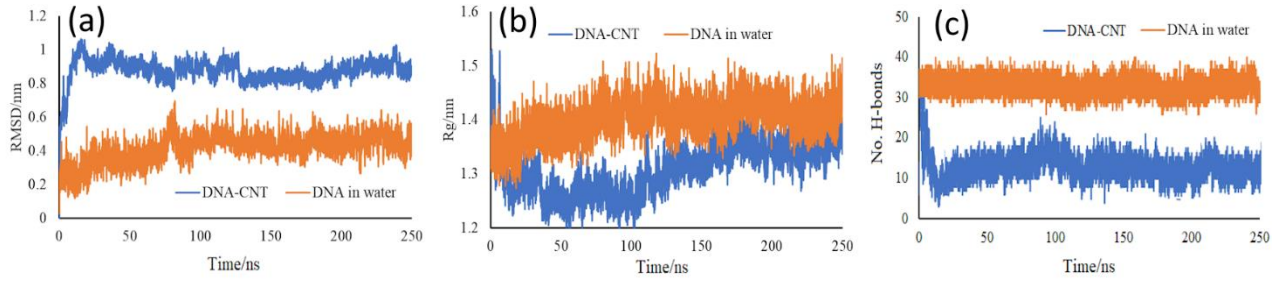

Figure 3: (a) RMSD, (b) Rg, and (c) intramolecular H-bonds for dsDNA during the two 250 ns MD simulation trajectories.

In the absence of the swCNT, the dsDNA system exhibited a certain number of stable intramolecular hydrogen bonds, indicative of the intact double stranded structure. However, with the introduction of the swCNT, a noticeable reduction in the number of these bonds was observed.

This decline supports the notion that the swCNT plays a role in destabilizing the hydrogen bond network between the dsDNA strands, contributing to the unwinding the double strands.

The decrease in intramolecular hydrogen bonds is particularly striking, dropping from 34 in the pure dsDNA in water system to around 10 in the final steps of the dsDNA-swCNT simulation. This drastic reduction further underscores the pronounced denaturing influence of the swCNT on the dsDNA structure.

To comprehend the dynamic adsorption process of swCNT on dsDNA, we closely examined the distance between the center of mass of the dsDNA segment and the swCNT. Figure 4a illustrates the dynamic changes in this distance, revealing a notable reduction from the initial 0.77 nm to approximately 0.29 nm.

Simultaneously, we investigated the contact area between the swCNT and dsDNA, crucial for characterizing the dynamic process of swCNT-dsDNA interaction (Figure 4b). The contact area, a pivotal parameter, is defined as half of the difference between the sum of solvent accessible surface areas (SASA) of dsDNA and swCNT and the SASA of the dsDNA-swCNT composite structure. Mathematically expressed as:

$$\text{Contact Area} = 1/2 \times (\text{SASA}_{\text{DNA}} + \text{SASA}_{\text{CNT}} - \text{SASA}_{\text{Complex}}) \quad (1)$$

As the distance between dsDNA and swCNT decreased during the initial 15 ns, with the swCNT eventually aligning along the central axis of the dsDNA, a noteworthy trend in the contact area emerged. The contact area increased from about 4.88 nm^2 to approximately 7.75 nm^2 during this phase and remained relatively stable thereafter until the end of the simulation. This stabilization indicates that the adsorption process reached a steady state.

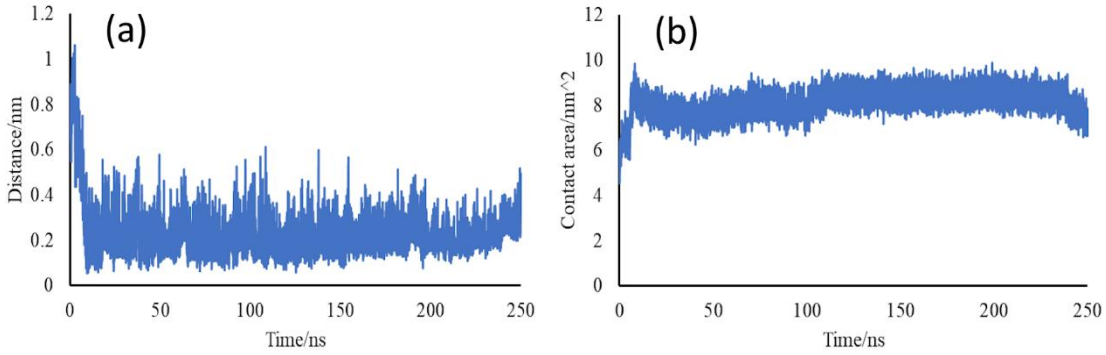

Figure 4: (a) The distance versus time between centers of mass of dsDNA segment and swCNT. (b) The contact surface area between dsDNA segment and swCNT.

The fixed distance between the centers of mass after 15 nanoseconds reflects positional stability between the swCNT and dsDNA, while the continued fluctuations in the RMSD until 130 nanoseconds indicate ongoing conformational adjustments within the dsDNA-swCNT complex. These two phenomena coexist because the distance analysis only captures global movement between the components, while RMSD accounts for finer-scale structural changes that take longer to equilibrate.

The observed reduction in distance between dsDNA and swCNT, coupled with the simultaneous increase in contact area, signifies a dynamic and intricate adsorption process. The initial approach and subsequent stabilization suggest the establishment of a stable state of adsorption, highlighting the dynamic equilibrium achieved between the swCNT and dsDNA.

Analyzing the contact area provides a quantitative measure of the interaction, showcasing the extent to which the swCNT becomes integrated into the dsDNA structure. This detailed

understanding of the dynamic adsorption process lays the foundation for elucidating the molecular and atomic details governing the stability and interactions within the swCNT-dsDNA complex.

To chronicle the dynamic interaction process between the dsDNA segment and the swCNT, we extracted configuration diagrams at various critical moments throughout the simulation process (Figure 5). The snapshots illustrate key stages in the evolving dynamics of the swCNT-dsDNA complex.

During the initial 15 ns of the MD simulation, a notable repositioning of the swCNT was observed. The CNT transitioned from the minor groove of the DNA to the central axis of the double-strand helix, initiating the denaturation process of dsDNA. This process persisted until approximately 80 ns, during which we observed a significant adjustment of the swCNT within the dsDNA structure. Between 80 and 130 ns, the swCNT fine-tuned its positioning within the dsDNA, marking a critical phase in the denaturation evolution. Although the denaturation process continued slightly until the end of the trajectory, this period showcased the intricate interplay between the swCNT and dsDNA, emphasizing the dynamic nature of their interaction.

In our investigation, we also quantified the van der Waals (vdW) energy between the dsDNA segment and the swCNT. As the swCNT was uncharged, electrostatic energy could not be extracted. Figure 6 illustrates three significant changes in vdW energy during the simulation. The initial shift occurred within the first 15 ns, where the vdW energy rapidly dropped to approximately -450 kJ/mol. Corroborating this with the changes in the configuration diagram in Figure 5, it becomes evident that during this period, the swCNT moved to the central axis of the dsDNA, initiating new interactions with the bases of the dsDNA segment. This sudden change in vdW energy reflects the onset of these interactions.

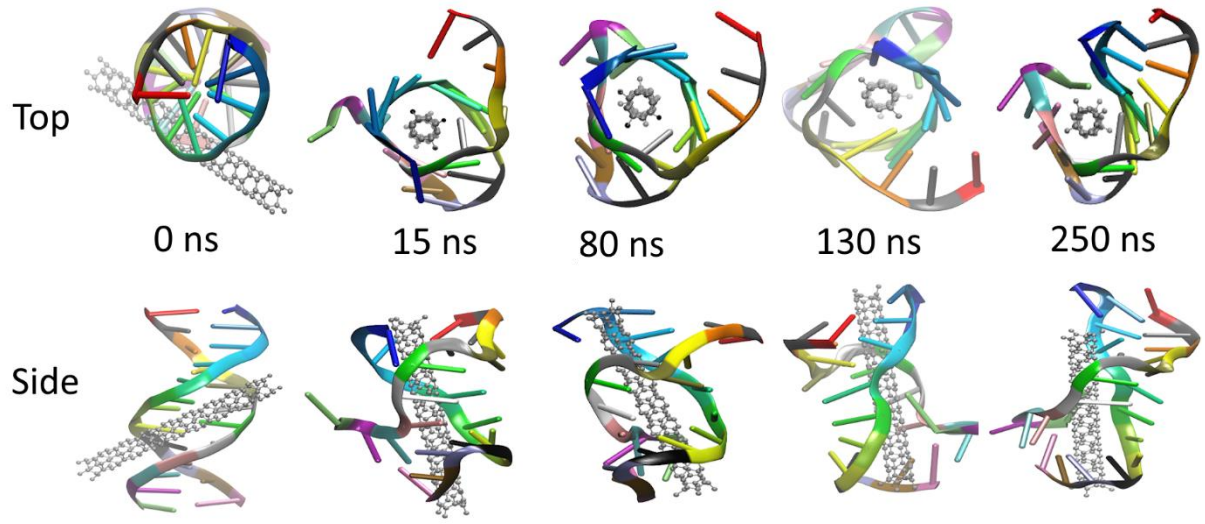

Figure 5: Top and side views of dsDNA-swCNT complex during 250 ns of trajectory.

The second transition unfolded between 15 to 130 ns, marked by another mutation in vdW energy. Correspondingly, the configuration diagram in Figure 5 reveals additional changes in the dsDNA structure as it adapts to its partially denatured state. Notably, during this timeframe, new bases were adsorbed to the surface of the swCNT, forming additional interactions. Subsequently, the vdW energy of the dsDNA segment and swCNT stabilized, fluctuating around -600 kJ/mol after reaching equilibrium.

Simultaneously, Figure 6 showcases the vdW energy of each base type in dsDNA with swCNT. Interestingly, the average vdW energy of DC bases stood out as significantly higher (more negative) than that of other bases. This observation suggests that DC bases were the most effective in interacting with the swCNT, and their interactions played a crucial role in the denaturation of dsDNA induced by the swCNT.

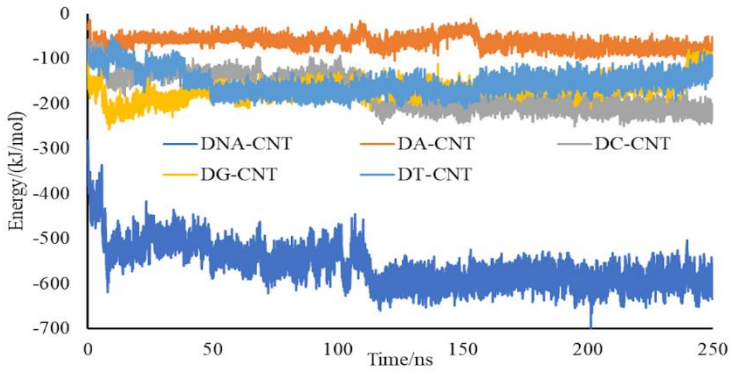

Figure 6: Van der Waals interaction energy between a dsDNA segment and each of its base types with the swCNT.

The initial interaction observed in Figure 6 is due to the use of docking results as the starting configuration for MD simulations. The initial binding affinity from docking ensures that dsDNA and swCNT are already interacting before the dynamic simulation begins. This does not detract from the validity of the MD results but instead highlights the fact that the system was designed to study the dynamics of an already formed complex.

In the case of swCNT and dsDNA, both are large, extended molecules with electron-rich regions. The carbon atoms of the swCNT form a continuous π-electron cloud due to its sp^2 hybridization, which interacts with the π-electron cloud of the nucleobases in dsDNA. These interactions are primarily non-covalent and are dominated by van der Waals forces.

From an atomic and molecular perspective, the vdW interactions between swCNT and dsDNA can be understood through the following mechanisms: i) One of the key contributors to vdW interactions is π-π stacking between the conjugated π-electron system of the swCNT and the aromatic nucleobases of dsDNA; ii) Both dsDNA and swCNT have hydrophobic surfaces,

particularly the carbon atoms of the swCNT and the aromatic rings of the nucleobases. The exclusion of water molecules from these surfaces can enhance the van der Waals interactions by promoting close contact between the swCNT and the dsDNA, maximizing the interaction surface area; iii) Since van der Waals forces are short-range interactions that decay with distance, the proximity of the swCNT to the dsDNA is a critical factor. The interaction energy increases (more negative values) as the swCNT approaches and fits into the major groove of dsDNA, allowing the atomic-scale forces to manifest more strongly.

In our simulations, we observed that the swCNT stabilizes within the major groove of dsDNA, maintaining close proximity that is within the range conducive for vdW forces (~3.4–4.0 Å; Figure 4a). This close contact provides strong evidence for vdW-driven stabilization of the complex.

3.3. Free energy of dsDNA-swCNT interaction

The dynamic equilibrium between the formation and decomposition of biomolecule-ligand complexes often occurs over time scales much longer than those accessible by typical MD sampling, which is limited to hundreds of ns. Consequently, thermodynamic parameters such as the activation energy barrier and the free energy of the binding reaction for complex formation can be challenging to estimate with conventional MD sampling. An alternative method for calculating the binding energy is the determination of the potential of mean force (PMF).

The resulting PMF profiles at 300 K, depicted in Figure 7, provide crucial insights into the thermodynamic feasibility of the dsDNA-swCNT interaction. The complex behavior of the PMF profile reveals multiple local energy minima, reflecting distinct intermediate states in the binding process of the swCNT with dsDNA: i) First Local Minimum at 1.48 nm: This first local minimum

likely corresponds to a partially bound state, where the swCNT is in close proximity to the major groove of dsDNA but has not fully penetrated or stabilized within it. At this distance, the swCNT may be interacting primarily with the outer regions of the DNA structure, exerting van der Waals and possibly some electrostatic forces. This state reflects a metastable interaction where the swCNT has encountered resistance from the dsDNA but remains loosely bound. ii) Second Local Minimum at 1.00 nm: The second local minimum suggests that the swCNT has partially inserted into the major groove of dsDNA, where more intimate contact between the swCNT and the dsDNA backbone is established. This state is more stable than the first minimum due to increased surface contact and stronger van der Waals interactions, but the system still needs to overcome a modest energy barrier to reach its global minimum. iii) Global Minimum at 0.75 nm: Reaching the global energy minimum at 0.75 nm indicates that the swCNT has fully embedded within the major groove of the dsDNA, achieving the most thermodynamically stable configuration (Figure 2). At this point, the swCNT forms extensive van der Waals contacts with the DNA, leading to a substantial reduction in the free energy of the system. This final bound state suggests maximal interaction between the swCNT and the dsDNA structure. The energy barrier of ~3.23 kJ/mol that must be overcome to achieve this state represents the energy required for the swCNT to fully insert and stabilize within the DNA groove.

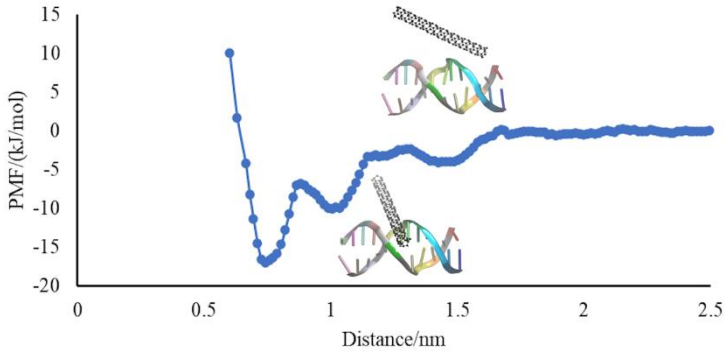

Figure 7: The PMF profile for the interaction of dsDNA-swCNT.

3.4. Other alteration in dsDNA following the structural changes

To assess the additional influences of swCNT on dsDNA, we examined the binding of Ethidium Bromide (EB) as a representative small molecule before and after dsDNA-swCNT interaction using molecular docking method. The unaffected dsDNA structure exhibited an affinity of about -9.1 kcal/mol for EB, indicative of EB intercalation into the dsDNA structure (Figure 8a). However, analysis of the denatured dsDNA structure, extracted from the final frame of our MD simulation, revealed a decreased affinity for EB, approximately to -7.9 kcal/mol (Figure 8b).

This observed decrease in binding affinity underscores a profound alteration in the dsDNA's ability to interact with specific drugs or small molecules post-swCNT interaction. Similar effect might be seen during the interaction of human dsDNA with the biomolecules which are essential for gene expression and replication. This phenomenon can somewhat justify the genomic toxicity mechanism of swCNTs.

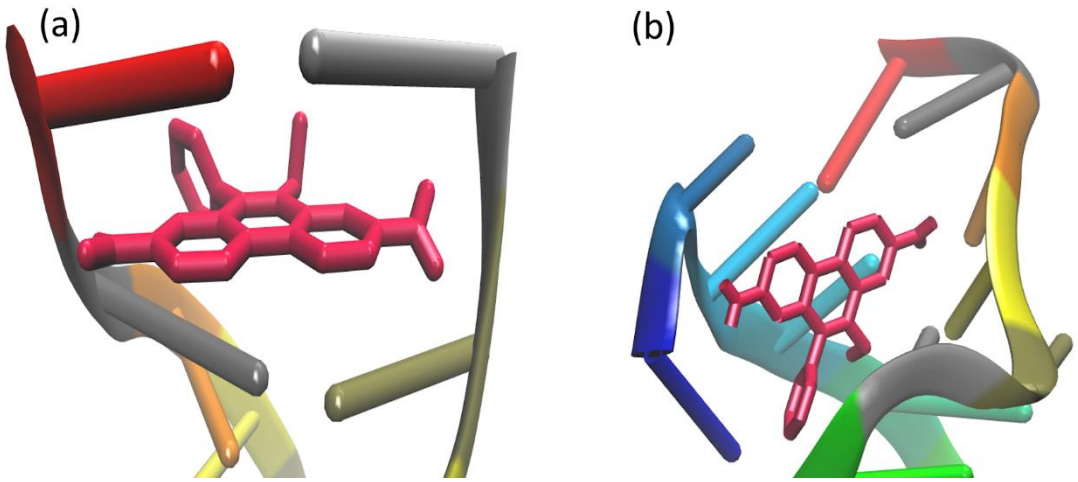

Figure 8: Binding poses of EB on dsDNA structures (a) unaffected dsDNA and (b) denatured dsDNA.

4. Conclusions

This study presents a detailed exploration of the interactions between single-walled carbon nanotubes (swCNTs) and double-stranded DNA (dsDNA) using an integrated molecular docking and molecular dynamics (MD) simulation approach. By examining various swCNT parameters—such as length, radius, and chirality—we uncover how these characteristics shape the binding affinity and structural stability of the dsDNA-swCNT complex. Our findings provide new insights into the toxicological implications of swCNTs, particularly in their ability to destabilize dsDNA at the molecular level.

The molecular docking results, which identified a zigzag swCNT (0.16 Å radius and 38 Å length) as having the highest binding affinity with dsDNA (-23.9 kcal/mol), serve as a precursor to the in-depth MD analyses. The MD simulations reveal that increasing the size of the swCNT, beyond a certain threshold, does not necessarily enhance binding affinity—offering a nuanced perspective on size-related effects. Additionally, the potential of mean force (PMF) profiles demonstrate the thermodynamic favorability of the dsDNA-swCNT interaction, exposing distinct energy barriers that govern the binding and unbinding process. These insights not only deepen our understanding of the interaction dynamics but also emphasize the denaturing effects swCNTs exert on dsDNA, as evidenced by reduced intramolecular hydrogen bonds and destabilization of the dsDNA structure.

A particularly noteworthy finding is the decreased binding affinity of Ethidium Bromide (EB) to dsDNA following its interaction with swCNT. This suggests that swCNTs may alter the binding of small molecules to DNA, highlighting a broader toxicological concern regarding nanomaterial exposure and its impact on biological systems.

This study contributes to the growing body of knowledge regarding the biological impacts of nanomaterials, particularly in the context of potential DNA damage and denaturation caused by swCNTs. The ability of swCNTs to interfere with DNA structure and the binding of essential small molecules like EB underscores the importance of investigating their toxicological effects further. The findings have important implications for the development of nanomaterial safety regulations and guidelines, particularly in fields where CNTs may be used in medical or environmental applications.

Looking forward, future studies could delve deeper into the electronic properties of dsDNA-swCNT complexes to better understand how these interactions influence their biological activity

and toxicity. This knowledge will be crucial for assessing the broader relevance of swCNTs across fields such as biomedicine, environmental science, and nanotechnology. By highlighting these broader implications, this study opens new avenues for exploring the safe and effective integration of nanomaterials into various technological applications.

Acknowledgement

This work was performed in SimatLab, a joint public-private laboratory dedicated to the multi-scale modelling of polymer materials. This laboratory is supported by Michelin, Clermont Auvergne University (UCA), CHU of Clermont-Ferrand and CNRS. We are also grateful to the Mesocenter Clermont Auvergne University for providing computing and storage resources.

References

[1] P. Karthik, A. Himaja, S. P. Singh, Carbon-allotropes: synthesis methods, applications and future perspectives, Carbon Lett. 15 (4) (2014) 219–237.

[2] B.O. Murjani, P.S. Kadu, M. Bansod, S.S. Vaidya, M.D. Yadav, Carbon nanotubes in biomedical applications: current status, promises, and challenges, Carbon Lett. 32 (2022) 1207–1226.

[3] M.L. Di Giorgio, S. Di Bucchianico, A.M. Ragnelli, P. Aimola, S. Santucci, A. Poma, Effects of single and multi walled carbon nanotubes on macrophages: cyto and genotoxicity and electron microscopy, Mutat. Res. Gen. Toxicol. Environ. Mutagen. 722 (2011) 20-31.

[4] D. Mohanta, S. Patnaik, S. Sood, N. Das, Carbon nanotubes: Evaluation of toxicity at biointerfaces, J. Pharm. Anal. 9 (5) (2019) 293-300.

[5] J.S. Kim, K.S. Song, I.J. Yu, Evaluation of in vitro and in vivo genotoxicity of single-walled carbon nanotubes, Toxicol. Ind. Health, 31 (2015) 747-757.

[6] M. Mrakovcic, C. Meindl, G. Leitinger, E. Roblegg, E. Frohlich, Carboxylated short single-walled carbon nanotubes but not plain and multi-walled short carbon nanotubes show in vitro genotoxicity, Toxicol. Sci. 144 (2015) 114-127.

[7] J. Lan, N. Gou, C. Gao, M. He, A.Z. Gu, Comparative and mechanistic genotoxicity assessment of nanomaterials via a quantitative toxicogenomics approach across multiple species, Environ. Sci. Technol. 48 (2014) 12937-12945.

[8] V. Raffa, G. Ciofani, O. Vittorio, C. Riggio, A. Cuschieri, Physicochemical properties affecting cellular uptake of carbon nanotubes, Nanomedicine 5 (1) (2010) 89–97.

[9] D. Mohanta, S. Patnaik, S. Sood, N. Das, Carbon nanotubes: Evaluation of toxicity at biointerfaces, J. Pharm. Anal. 9 (5) (2019) 293–300.

[10] T. Jiang, C. A. Amadei, N. Gou, Y. Lin, J. Lan, C. D. Vecitis, A. Z. Gu, Toxicity of single-walled carbon nanotubes (swcnts): effect of lengths, functional groups and electronic structures revealed by a quantitative toxicogenomics assay, Environ. Sci. Nano 7 (5) (2020) 1348–1364.

[11] J. Cheng, K. S. Fernando, L. M. Veca, Y.-P. Sun, A. I. Lamond, Y. W. Lam, S. H. Cheng, Reversible accumulation of pegylated single-walled carbon nanotubes in the mammalian nucleus, Acs Nano 2 (10) (2008) 2085–2094.

[12] S. Barua, S. Mitragotri, Challenges associated with penetration of nanoparticles across cell and tissue barriers: a review of current status and future prospects, Nano Today 9 (2) (2014) 223–243.

[13] N. W. S. Kam, Z. Liu, H. Dai, Carbon nanotubes as intracellular transporters for proteins and dna: an investigation of the uptake mechanism and pathway, Angew. Chem. Int. Ed. 45 (4) (2006) 577–581.

[14] W. Tutak, K. H. Park, A. Vasilov, V. Starovoytov, G. Fanchini, S.- Q. Cai, N. C. Partridge, F. Sesti, M. Chhowalla, Toxicity induced enhanced extracellular matrix production in osteoblastic cells cultured on single-walled carbon nanotube networks, Nanotechnology 20 (25) (2009) 255101.

[15] M.-C. F. Jaurand, A. Renier, J. Daubriac, Mesothelioma: Do asbestos and carbon nanotubes pose the same health risk?, Part. Fibre Toxicol. 6 (1) (2009) 1–14.

[16] A. Casey, E. Herzog, F. Lyng, H. Byrne, G. Chambers, M. Davoren, Single walled carbon nanotubes induce indirect cytotoxicity by medium depletion in a549 lung cells, Toxicol. Lett. 179 (2) (2008) 78–84.

[17] S. Tabari, Y. Jamali, R. Poursalehi, Multi-scale simulation of carbon nanotubes interactions with cell membrane: Dft calculations and molecular dynamic simulation, Proced. Mater. Sci. 11 (2015) 423–427.

[18] Y. Yu, H. Sun, K. Gilmore, T. Hou, S. Wang, Y. Li, Aggregated singlewalled carbon nanotubes absorb and deform dopamine-related proteins based on molecular dynamics simulations, ACS Appl. Mater. Interfaces. 9 (38) (2017) 32452–32462.

[19] R. Rasoolzadeh, F. Mehrnejad, M. Taghdir, P. Yaghmaei, Effects of single-walled carbon nanotube on the conformation of human hepcidin: molecular dynamics simulation and binding free energy calculations, J. Biomol. Struct. Dyn. 37 (8) (2019) 2125–2132.

[20] Y. Mahmoodi, F. Mehrnejad, K. Khalifeh, Understanding the interactions of human follicle stimulating hormone with single-walled carbon nanotubes by molecular dynamics simulation and free energy analysis, Eur. Biophys. J. 47 (2018) 49–57.

[21] M. Hosseinzadeh, S. Nikjoo, N. Zare, D. Delavar, S. Beigoli, J. Chamani, Characterization of the structural chagaes of human serum albumin upon interaction with single-walled and multi-walled carbon nanotubes: spectroscopic and molecular modeling approaches, Res. Chem. Intermed. 45 (2019) 401–423.

[22] M. Sahihi, G. Borhan, The effects of single-walled carbon nanotubes (swcnts) on the structure and function of human serum albumin (hsa): Molecular docking and molecular dynamics simulation studies, Struct. Chem. 28 (2017) 1815–1822.

[23] W. Humphrey, A. Dalke, K. Schulten, VMD – Visual Molecular Dynamics, J. Mol. Graph. 14 (1996) 33–38.

[24] G. M. Morris, R. Huey, W. Lindstrom, M. F. Sanner, R. K. Belew, D. S. Goodsell, A. J. Olson, Autodock4 and autodocktools4: Automated docking with selective receptor flexibility, J. Comput. Chem. 30 (16) (2009) 2785–2791.

[25] G. M. Morris, D. S. Goodsell, R. S. Halliday, R. Huey, W. E. Hart, R. K. Belew, A. J. Olson, Automated docking using a lamarckian genetic algorithm and an empirical binding free energy function, J. Comput. Chem. 19 (14) (1998) 1639–1662.

[26] W. L. Jorgensen, J. Chandrasekhar, J. D. Madura, R. W. Impey, M. L. Klein, Comparison of simple potential functions for simulating liquid water, J. Chem. Phys. 79 (2) (1983) 926–935.

[27] D. J. Evans, B. L. Holian, The nose–hoover thermostat, J. Chem. Phys. 83 (8) (1985) 4069–4074.

[28] M. Parrinello, A. Rahman, Polymorphic transitions in single crystals: A new molecular dynamics method, J. Appl. Phys. 52 (12) (1981) 7182– 7190.

[29] A. Rahman, F. H. Stillinger, Molecular dynamics study of liquid water, J. Chem. Phys. 55 (7) (1971) 3336–3359.

[30] S. Ur Rehman, T. Sarwar, M.A. Husain, H.M. Ishqi, M. Tabish, Studying non-covalent drug–DNA interactions, Arch. Biochem. Biophys. 576 (2015) 49-60.

[31] U. Essmann, L. Perera, M. L. Berkowitz, T. Darden, H. Lee, L. G. Pedersen, A smooth particle mesh ewald method, J. Chem. Phys. 103 (19) (1995) 8577–8593.

[32] T. Darden, D. York, L. Pedersen, Particle mesh ewald: An n log (n) method for ewald sums in large systems, J. Chem. Phys. 98 (12) (1993) 10089–10092.

[33] B. Hess, H. Bekker, H. J. Berendsen, J. G. Fraaije, Lincs: A linear constraint solver for molecular simulations, J. Comput. Chem. 18 (12) (1997) 1463–1472.

[34] H. J. Berendsen, D. van der Spoel, R. van Drunen, Gromacs: A messagepassing parallel molecular dynamics implementation, Comput. Phys. Commun. 91 (1-3) (1995) 43–56.

[35] E. Lindahl, B. Hess, D. Van Der Spoel, Gromacs 3.0: a package for molecular simulation and trajectory analysis, J. Mol. Model. 7 (2001) 306–317.

[36] H. Berendsen, B. Hess, E. Lindahl, D. Van Der Spoel, A. Mark, G. Groenhof, Gromacs: fast, flexible, and free, J. Comput. Chem 26 (16) (2005) 1701–1718.

[37] M. J. Abraham, T. Murtola, R. Schulz, S. P´all, J. C. Smith, B. Hess, E. Lindahl, Gromacs: High performance molecular simulations through multi-level parallelism from laptops to supercomputers, Softwarex 1 (2015) 19–25.

[38] T. E. Cheatham III, D. A. Case, Twenty-five years of nucleic acid simulations, Biopolymers 99 (12) (2013) 969–977.

[39] J. S. Hub, B. L. De Groot, D. van der Spoel, g wham a free weighted histogram analysis implementation including robust error and autocorrelation estimates, J. Chem. Theory Comput. 6 (12) (2010) 3713–3720.